



Metal-Molecule Schottky Junction Effects in Surface Enhanced Raman Scattering

M. R. Gartia, T. C. Bond and G. L. Liu

July 23, 2010

Nanotechnology

Disclaimer

This document was prepared as an account of work sponsored by an agency of the United States government. Neither the United States government nor Lawrence Livermore National Security, LLC, nor any of their employees makes any warranty, expressed or implied, or assumes any legal liability or responsibility for the accuracy, completeness, or usefulness of any information, apparatus, product, or process disclosed, or represents that its use would not infringe privately owned rights. Reference herein to any specific commercial product, process, or service by trade name, trademark, manufacturer, or otherwise does not necessarily constitute or imply its endorsement, recommendation, or favoring by the United States government or Lawrence Livermore National Security, LLC. The views and opinions of authors expressed herein do not necessarily state or reflect those of the United States government or Lawrence Livermore National Security, LLC, and shall not be used for advertising or product endorsement purposes.

Metal-Molecule Schottky Junction Effects in Surface Enhanced Raman Scattering

Manas Ranjan Gartia¹, Tiziana C. Bond² and Gang Logan Liu^{3,*}

¹Department of Nuclear, Plasma and Radiological Engineering, University of Illinois, Urbana-Champaign, IL, 61801, USA

²Center for Micro and Nanotechnology, Lawrence Livermore National Laboratory, 7000 East Avenue, Livermore, CA 94550

³ Micro and Nanotechnology Laboratory, Department of Electrical and Computer Engineering, University of Illinois, Urbana-Champaign, IL, 61801, USA

*CORRESPONDING AUTHOR: Gang Logan Liu (loganliu@illinois.edu)

ABSTRACT

We propose a complementary interpretation of the mechanism responsible for the strong enhancement observed in Surface Enhanced Raman Scattering (SERS). The effect of a strong static local electric field due to Schottky barrier at the metal-molecule junction on SERS is systematically investigated. The study provides a viable explanation to the low repeatability of SERS experiments as well as the Raman peak shifts as observed in SERS and raw Raman spectra. It was found that strong electrostatic build-in field at the metal-molecule junction along specific orientations can result in 2-4 more orders of enhancement in SERS.

1. Introduction

Since its discovery [1-3], Surface Enhanced Raman Scattering (SERS) is progressively breaking new grounds and now even applied for the detection of more complex molecules and biologically relevant materials [4]. The single molecule detection capability [5, 6] has enhanced the prospect of using Raman probe in sensor application [7-9], hazardous materials detection [10, 11] and more recently, probing biological structures [12, 13]. Over the years three possible mechanisms for enhancement in Raman scattering have been identified [14]: (i) the surface plasmon resonance in the metal particle (or Electromagnetic mechanism) [2,3, 15-19] (ii) a charge transfer resonance involving transfer of electrons between the molecule and metal energy level (or simply Charge Transfer mechanism) [16, 20-27] (iii) resonance within the molecule itself [14]. The well known electromagnetic (EM) mechanism can be described as follows: when the incident laser frequency (or wavelength) is in resonance with the plasmon mode of the nanoparticle, a large amount of energy can be “concentrated” by the nanoparticle [28]. Subsequently the nanoparticle re-emits a portion of the EM energy by Mie scattering, thereby creating an intense surface field with very high energy density at or near the particle surface. In general, EM enhancement should amplify the Raman scattering non-selectively irrespective of type of molecules adsorbed on a particular surface [29]. However, the molecules CO and N₂ differ by a factor of 200 in

their SERS intensities under the same experimental conditions [26]. Another interesting example is that of water. While many SERS studies are conducted in aqueous systems, there is rarely an enhancement in the Raman spectrum of water. These results cannot be explained by invoking only electromagnetic enhancement. Further, when the coupling of chemical enhancement effect of the nanoparticles is considered, the EM enhancement of SERS can be up to the order of 10^{10} [30]. The huge enhancement factor (10^{14} - 10^{15}) as seen in many single-molecule experiments are normally attributed to the low concentration level of the analyte in SERS experiments and hence, mainly due to the difference in the number of molecules showing scattering in SERS as compared to bulk Raman [31]. However, the contribution from electromagnetic coupling and chemical binding are clearly inseparable in experiments due to the fact that the SERS detection itself depends on the electromagnetic enhancement process [32]. Thus the kind of charge transfer (CT) contribution in those high enhancement experiments (10^{14} - 10^{15}) is still unknown. In the charge transfer model [33], an incident photon excites an electron from the metal surface into an adsorbed molecule, creating a negatively charged excited molecule. The molecular geometry of this excited molecule differs from that of the neutral species. This charge transfer induces a nuclear relaxation within the excited molecule, which results in, the return of the electron to the metal surface, the creation of an excited neutral molecule and the emission of a wavelength shifted (Raman) photon [18]. In principle in the CT an adsorbed molecule can, under specific conditions, interact with a metal surface in such a way that there is a large increase in molecular polarizability (change), α . Further, it was shown experimentally that the charge transfer can occur in both directions (that is, metal cluster-to-molecule or molecule-to-metal cluster) depending on the relative energies of the metal Fermi level and the HOMO (highest occupied molecular orbital) and LUMO (lowest unoccupied molecular orbital) levels of the adsorbed molecule [22]. For example, molecules with low-lying unfilled π -orbitals (such as pyridine) experienced metal-to-molecule transfer, while those without low-lying unfilled orbitals (such as NH_3 or piperidine) tended to transfer electrons to the metal [14, 22].

It is also important to realize that the aforementioned three mechanisms are not independent of each other, but rather the total enhancement is due to the result of combine effect of one or more of the three

mechanisms depending on the wavelength used in the experiment and the specific adsorbate and metal [34]. Even though it may not always be possible to separate these different mechanisms experimentally or theoretically, certain limits can be established where one mechanism is more dominating than the others. In fact, to isolate the CT enhancement, SERS has been studied for adsorbates on smooth surfaces, which are known to be incapable of supporting large surface plasmons. These studies showed only small (10^1 - 10^2) enhancements [35, 36]. However, recent theoretical [37] as well as experimental [38, 39] studies has shown that under certain conditions the CT enhancement can be much larger than is usually predicted earlier. In addition, large SERS enhancements have also been observed for molecules interacting with small nanoclusters or nanocrystalline semiconductor surfaces, both of which are not expected to support plasmon resonances and thus should show only small EM enhancement [40-42]. Though, the CT mechanism has been widely studied and fairly gives an intuitive picture of the chemical enhancement, it mostly relies on phenomenological parameters [16, 24]. In this context, it is increasingly important to understand the microscopic nature of SERS using first principle modeling [43]. It is now widely believed that the chemical bonding effects in SERS can be simulated just by considering the local environment of a molecule which is also consistent with the adatom model [26, 44]. The adatom model assumes that the atomic-scale roughness features determine the hot spots on a metal surface and invariably discount the electromagnetic enhancement due to the excitation of surface plasmons in the metal as well as the effect of interference between the chemical and the electromagnetic mechanism if any. Indeed in such approach the CT and EM effects enter in multiplicative fashion in the total enhancement factor [45]. Also, in most of the previous theoretical studies of SERS, only a few metal atoms were used to model the molecule/surface interaction. For example, Aroca et al. [46] did the simulation with just a single silver atom to mimic the chemisorption of phthalimide on a silver surface and obtained a reasonable agreement with experiments. Similarly, resonance Raman calculation [47], SERS study of pyridine adsorbed on silver clusters [34, 37, 48] and SERS simulation for benzenethiol adsorbed on Ag surface [44] have been performed with fair success by using a few tens of atoms. It has also been shown using rigorous density functional theory (DFT) computation by using large surface unit cells, that the ($\sqrt{3} \times \sqrt{3}$) unit cell is sufficient to treat the single molecule adsorption of benzenethiol on

Au (1 1 1) surface in the low coverage limit [49]. A full coverage can be defined as one thiol molecule per three Au surface atoms, which is consistent with our simulation approach. The STM experiments for structure of benzenethiol adsorbed on gold (111) showed surface coverage of about 0.306 for the benzenethiol molecule [50]. In this paper, simulations for chemical bonding effects on Raman scattering have been performed for benzenethiol using 1-3 gold atoms.

The various issues considered so far in the context of chemical enhancement includes the binding geometry of the adsorbate [51], the effects of adsorption on various noble and transition metal surfaces [52], the influence of positively charged atoms at the metal surface [53, 54], the effect of adsorbed chloride anions [55], the effect of nonzero static electric fields [56], and the solvent effects in the calculations [57]. Although there is clear evidence of the existence of a solid-liquid electrochemical interface (electric double layer) in all aqueous SERS experiment as well as metal-molecule interface in non-aqueous SERS experiments, there is no systematic study so far to elucidates these effects. It is also well known that the strong electric field present at such an interface perturbs the vibrational frequencies of the adsorbed species—the vibrational Stark effect (VSE) [1, 58]. In addition, the electric field also changes the adsorbate vibrational line strength—the vibrational intensity effect (VIE) [59, 60]. Here we present a systematic study of both of these effects on a model SERS molecule, Benzenethiol, by assuming an interfacial static electric field between metal-molecule interface whose magnitude and direction are taken as parameters of the model. The external static electric field can be seen as a perturbation to the system Hamiltonian. Our present computational approach is also motivated by the goal of interpretation of potential dependent SERS studies [61, 62]. In recent experiment, an enhancement of the order of 10^5 - 10^9 was observed upon application of external electric field to glutamic acid adsorbed on Ag substrate [63]. The present study aims to provide a microscopic insight to any such studies and may lead to achieving applied electric field controllable SERS intensity module. To present a simplified picture of metal-molecule interface, the molecule has been considered as a semiconductor (the justification is described below) and the magnitude of the static electric field so developed is calculated based on metal-molecule Schottky barrier mechanism.

Molecule as semiconductor

Most organic materials are electrical insulators with values of electrical conductivity at room temperature in the range 10^{-9} - 10^{-14} S cm⁻¹ [64] (10^9 - 10^{14} Ω cm resistivity). To obtain a larger conductivity and hence semiconducting behaviour, the HOMO–LUMO gap needs to be reduced; this can be achieved with extensive π -bonding. This reduced band gap allows electrons to more easily jump between conduction and valence bands and gives rise to the semiconductive properties [65]. In crystalline semiconductor technologies, n-type and p-type refer to the type of dopant, and therefore majority carrier, in a semiconductor. In crystalline materials both holes and electrons can usually be transported reasonably well. It is, nevertheless, common in the literature to refer to hole transporting disordered (doped) semiconductor materials as p-type and electron transporting materials as n-type because this describes their majority carriers and semiconducting behavior.

On the other hand, aromatic rings contain alternating single and double bonds that lead to overlapping p-orbitals, which form π -bonds. In π -bonds, electrons delocalize and are shared between the atoms on the ring's backbone. Similar to conduction due to a delocalized “sea of electrons” in metals, free movement of delocalized π -electrons in organic compounds allows organic molecules to conduct electricity and behave as semiconductors [66]. Then how to distinguish p-type or n-type organic semiconductor? In view of popular organic semiconductor field, electron-rich conjugated polymers are termed as p-type and electron-poor ones are termed as n-type [67]. For example, in benzenethiol, the hydrogen atoms which surround the carbon backbone are less electronegative than the carbon backbone itself and lend some electron density to the delocalized π -electron cloud. The electron rich conjugated molecule has difficulty accepting another electron, but is able to lose an electron with relative ease. As a consequence, positive charge carriers expected to dominate transport in benzenethiol molecule [66]. In other words, molecules involving π -conjugation have high HOMO levels and exhibit electron-donating properties. Hence, these molecules are good candidates for p-type semiconductors [68].

However, it should be recognized here that the view of holes and electrons pi-orbital molecule as free carriers is rather simplistic. It allows us to make some general predictions about the trends in energy levels if we use it carefully, but may not extend well to all polymers [66]. It should also be recognized

that the expected carrier mobility in such organic semiconductor is typically low ($\sim 1 \text{ cm}^2\text{V}^{-1}\text{s}^{-1}$) as compared to traditional inorganic semiconductors (for silicon crystal $\sim 300\text{-}900 \text{ cm}^2\text{V}^{-1}\text{s}^{-1}$).

Metal-Molecule interface

It is well known that a potential barrier known as Schottky barrier forms at a metal-semiconductor junction [69, 70] and the build-in electrostatic field strength can be as high as a few volts per angstrom. The formation of Schottky barrier between metal electrode and organic electronics materials has been extensively studied both theoretically [71-73] and experimentally [74-77] in recent years. In addition, the application of SAMs (Self Assembled Monolayers) of π -conjugated thiols for single-molecule electronics have been extensively studied [78]. Herein we assume the benzenethiol molecule is equivalent to a highly doped p-type semiconductor and the gold-benzenethiol junction is equivalent to a metal-semiconductor Schottky barrier junction as shown in Fig. 1 (a). Providing a self-assembly monolayer coverage of $6.8 \times 10^{14} \text{ cm}^{-2}$ for benzenethiol on gold surface [79, 80], the packing density of benzenethiol or equivalently the electron donor concentration can be calculated to be $N_D = 1.36 \times 10^{22} \text{ cm}^{-3}$.

The depletion width at the metal-molecule junction can be calculated using the relation $W = \left[\frac{2\epsilon_s \phi_s}{qN_D} \right]^{1/2}$

where ϵ_s is the permittivity of benzenethiol molecule, ϕ_s is the surface potential, q is the fundamental electric charge. The maximum surface potential ϕ_s is approximated as half of the energy band gap of the benzenethiol molecule, which is about 2 eV. Taking relative permittivity (ϵ_r) of benzenethiol as 4.38 [81] the depletion width of our system was thus found to be 2.88 Å. The build-in electric field was calculated using the simple relation $E_0 = \frac{qWN_D}{\epsilon}$ and found to be 1.41 V/Å. It should be noted that this estimated electric field strength is the maximum value and the real build-in electric field should be slightly lower than this value. Figure 1 (b) displays the schematic of the energy-band diagram of a gold/benzenethiol Schottky junction, using the parameters obtained in our analysis. The work function of Au is 5.3 eV [82], the ionization potential (IP) of benzenethiol is 8.32 eV [83, 84]. The band gap of benzenethiol was calculated to be 4.1 eV. The difference between Fermi energy of metal and HOMO

(highest occupied molecular orbital) is known as HIB (hole injection barrier) and difference in Fermi level and that of LUMO (lowest unoccupied molecular orbital) of organic molecule is known as EIB (electron injection barrier) [71, 77]. In the present study HIB is calculated to be ~ 2.06 eV and EIB is calculated to be ~ 2.04 eV.

Now, the interface between metal and organic semiconducting layers can be described with the help of screening parameter (S parameter) [85] which is defined as $S = \frac{d\phi_B^P}{d\phi_m}$, where ϕ_m and ϕ_B^P denote the work function of the metal and the barrier height for carrier injection at the interface for holes (HIB), respectively. $S = 0$ corresponds to the so called Bardeen limit for which Fermi level pinning occurs. Similarly, $S = 1$ corresponds to an ideal Schottky barrier at the interface (Schottky limit) [86]. For metal–organic molecule interfaces formed by chemical bonds, it is reasonable to interpret the Bardeen limit as the situation where strong orbital interactions between frontier orbitals of metals and the HOMO of molecule occurs and the Schottky limit as the situations where weak orbital interactions occurs between them. In other words, when molecules have large energy gaps between the HOMO and the LUMO, as in the present study, Schottky limit holds well [86]. In fact the value of S was calculated to be 0.5 experimentally for Au and benzenethiol system [86]. Again the density of states $D(E_F)$ of interfacial electronic states can be calculated using the relation, $S = (1 + e^2\delta D(E_F)/\epsilon)^{-1}$, [85-87] where e , δ , and ϵ denote the elementary charge, width of the metal–molecule interface, and dielectric constant, respectively. Taking δ and ϵ to be 5.7 Å and 4.38 for benzenethiol [81] respectively, $D(E_F)$ is estimated to be 4.2×10^{13} states/(cm²·eV), which is less than 20% of the density of states of Au at the Fermi level [88]. Even though small, the existence of a finite density of states for the frontier orbitals of the molecule near the Fermi level, indicates that electrons pass through hybrid orbitals composed of frontier orbitals of the metal and molecule supporting the charge transfer mechanism.

Computational approach and details

Using a simple model we have estimated the built-in electric field of the order of few $\text{V}/\text{\AA}^\circ$. The effect of such high built-in electric field on the molecular conformation, electronic and vibrational properties was probed using a quantum mechanical simulation. The theoretical simulations were performed using Density Functional Theory (DFT) implemented in Amsterdam Density Functional (ADF) program package [89, 90]. DFT methods are based on the Hohenberg-Kohn theorem which states that the ground state electronic energy of a molecule can be expressed exactly as the electron density of the molecule. The Becke-Perdew (BP86) XC-potential [91, 92] and a triple- polarized Slater type (TZP) basis set from the ADF basis set library were used in our simulation. The validity of using DFT and ADF for quantum mechanical SERS calculation has already been proven by many researchers [37-48]. Further, in the present study the validity of our results has been checked by comparing the computational results for the Raman as well as SERS spectra with the experimental results. The details of the experiments have been given elsewhere [93]. The simulated results match fairly well with the experiments as shown in Fig. 2. Comparison of results obtained from DFT study with experiments for neat Raman is shown in Fig. 2 (a). Similarly, the result for SERS spectra of benzenethiol calculated by DFT simulation and obtained from experiment is shown in Fig. 2 (b). Clearly the characteristics peaks observed in the experiments are captured by the DFT simulation.

Results and discussion

The polarization effect of SERS has already been observed in single molecule experiment [5] and recently been verified with a computational model [94]. Here, we investigate the effect of built-in electric field direction on the Raman scattering process. To model such a system, first a static electric field is applied on the benzenethiol molecule along various directions to simulate the built-in field of Schottky barrier developed at the metal-molecule junction. The molecular conformation under different conditions is found through the energy minimization process in each case. Here, all the directions are related to the molecular co-ordinates and hence positive Z-direction should be normal to the benzene ring structure. Figure 3(a) shows the deformation in chemical bond length of benzenethiol molecule due to application of electric fields. In general, it was found that the extent of the bond length change is proportional to the

build-in electric field. Depending on the relative orientations between the molecule and the build-in electric field, different trends show for the length change of various chemical bonds such as the carbon-sulfur bond and carbon6-sulfur bond. The largest change in bond length and dihedral angle was seen when the build-in field was perpendicular to the benzene ring (positive Z-direction). The dihedral bond angle also changes as shown in Fig 3(b). One can clearly see that the build-in field leads to a large variation in bond length and dihedral angle at specific orientations. To emphasize the change in bond orientation and length under application of electric field, the actual conformation of benzenethiol molecule is shown as obtained from our simulation in Fig. 3(c). The molecular conformation change will inherently induce dipole moment and polarizability changes since the inter-atomic distance and angle are altered (please see the supporting information). The direct correlation between the build-in electric field and the polarizability derivative of two dipoles in Benzenethiol molecule is shown in Fig. 3(d). These two dipoles correspond to the vibrational modes at 403 cm^{-1} and 1573 cm^{-1} respectively. The trend in the change of bond length and change in the polarizability is consistent with other theoretical prediction [37, 44].

The close-up of the peaks is also shown in the inset. The large enhancement of a peak in particular direction can be assigned to the largest change in the polarizability derivative in that direction. In the particular case shown here, for example, the largest change in polarizability derivative for 403 cm^{-1} peak is in +Z direction (perpendicular to benzene ring) and hence, the largest enhancement one could see for that peak is in +Z direction. Similarly, for 1573 cm^{-1} peak, the largest change in polarizability derivative observed was in +X direction (parallel to benzene ring structure). That's why the largest enhanced 1573 cm^{-1} peak corresponds to electric field applied in +X direction. For a similar molecule, Pyridine, Arenas et al. [95] found experimentally that the modes at 410, 598, 1204 and 1573 cm^{-1} shows the strongest dependence on the electrode potential. The theoretical TDDFT simulation for benzenethiol adsorbed on silver cluster shows similar trend [44] which is in agreement with current simulation results.

The graphical explanation for the effect of build-in field at the Schottky barrier on molecular dipole moment is shown in Fig. 4. The molecular quantum states can be described based on the Born-

Oppenheimer separation of nuclear and electronic degrees of freedom. The electrons are much lighter than nuclei and can adjust rapidly to the instantaneous nuclear configuration (which is also known as Franck-Condon principle). Therefore molecules are characterized by "potential energy surfaces" - plots of energy versus internuclear separation and there is a separate surface for each electronic configuration [96]. Figure 4 shows schematically that there must be an intermediate state created due to adsorption of benzenethiol to gold atoms as the excitation incident wave (532 nm or 2.33 eV) is far below the purely intramolecular electronic transitions level (4.1 eV) which is also supported by recent theoretical model [44]. The increase in polarizability derivative (and subsequent enhanced Raman intensity) can be explained by the large change in the dipole moment due to change in molecular conformation (and increase in the bond length as shown in Fig. 4) (please see supporting information for more details). The increased dipole moment ($p=qd$) is depicted by a larger separation of two charges described by red and blue color as observed for the HOMO level of benzenethiol. Since the polarizability of the molecule is related to the vibrational co-ordinates and the dipole moment, an increase in polarizability is expected. We also observed an increase in the absolute polarizability derivative (modulus of the polarizability derivative) along with increase in dipole moment (Fig. 3(d)). The Raman scattering cross-section is proportional to the square of polarizability derivative $\frac{d\sigma}{d\Omega} \propto \left(\frac{d\alpha}{dr}\right)^2$ [97]. Hence, an increase in Raman scattering cross-section is expected as a result of large change in polarizability derivative even in the absence of electronic transition.

The metal-molecule Schottky barrier also induces the change of energy band gap of Benzenethiol molecule. As shown in Fig. 5, the band gap of isolated benzenethiol molecule is in ultraviolet region which makes the electronic level transition forbidden for visible excitations. The Fermi (HOMO) level of gold is somewhere in the middle of the molecule energy band gap. The energy difference between gold Fermi level and HOMO of isolated molecule shows the viability of charge transfer scheme where charges can transfer from metal atom cluster to the molecule or from the molecule to the metal cluster. Due to attaching gold atoms the density and number of accessible states in the hybrid system increase. In addition, the band gap shrinks due to attachment of gold atoms which may make it possible to induce

resonance Raman for visible excitations. It should be noted that the band gap of benzenethiol calculated in the present study is 4.092 eV which is in close agreement to the value of 4.027 eV calculated by Morton and Jensen [34]. Similarly the band gap calculated in the present study for benzenethiol with three gold atoms configuration is 0.75 eV whereas for similar system the value calculated by Letardi and Cleri [98] was 0.76 eV. The prediction of shrinking band gap due to adsorption is also in good agreement with the theoretical study by Saikin et al. [44] for benzenethiol adsorbed on a silver cluster. The build-in electric field further shrinks the band gap, increasing the probability of transition to higher excited states and further enlarging the Raman scattering cross-section.

The reason for shrinkage of band gap (Fig. 6 (a) and (b)) due to adsorption to metal atoms can be described as follows. The ionic cores in the metal are assumed to give rise to a square potential well for the electrons and all states are filled up to the Fermi level, E_F [71]. The energy difference between E_F and the potential energy of an electron in the vacuum above this hypothetical surface, U_{vac} , is generally referred to as the *intrinsic* work function, Φ' , (or chemical potential) of the metal (e.g. for gold it is 5.3 eV) (Fig. 6 (c)). However, because the potential well is not infinitely deep, there is always a finite probability of finding electrons outside the potential well, that is, electron density is “leaking out” from the metal into the vacuum [99]. Consequently, a dipole layer is formed with a positively charged region below the surface (red region) and negatively charged region (light blue) just outside the metal surface. This dipole layer is commonly referred to as the *surface dipole* and gives rise to a potential step across the metal surface (Fig. 6 (d)) [71]. The surface dipole raises U_{vac} directly above the metal surface relative to E_F and leads to the *observed* work function, Φ , of the metal surface [99].

Now when a benzenethiol molecule appears near the metal surface, there exist a mismatch of ionization potential (IP \sim 8.32 eV) of the molecule and the work function of metal (\sim 5.3 eV). As we pointed out earlier, this will lead to a Schottky barrier which will give rise to a built-in electric field directed from metal surface to the organic molecule. The developed electric field will oppose further leakage of electrons from metal. So even for a weakly interacting (physisorbed or va der Waal interacting) species or for a strongly interacting (covalent bonded) species, the electron cloud leaking out of the metal

surface is pushed back into the metal (Fig. 6 (e)) [100]. This *push-back* (or *pillow*) effect always contributes to reduce the surface dipole and lower U_{vac} relative to E_{F} and, consequently, leads to a reduced work function, Φ_{mod} , of the sample [71]. The amount by which the surface dipole is reduced is generally known as the *interface dipole* [71]. The interface dipole is expected to lower the LUMO level of the organic molecule too. In the present study we have observed a reduction of ~ 2.54 eV for benzenethiol LUMO level. In addition, an interface dipole with its negative pole pointing toward the organic layer and its positive pole toward the metal is expected to increase the metal work function (i.e., decreases the Fermi energy) and increases the HOMO energy of the organic layer by adding an electrostatic energy [101]; as a result, the hole injection barrier (HIB) should be reduced (Fig. 6 (b) and (e)). In fact, in our simulation, we have observed an increase of 1.37 eV for the HOMO level of benzenethiol up on conjugation to gold which reduces the HIB from 2.06 eV before conjugation to 0.69 eV after conjugation.

To elucidate the effect of magnitude of build-in electric field on Raman intensity, the Raman scattering spectra are simulated by calculating the Raman intensity as the function of applied electric field. Figure 7 shows that with application of local build-in electric field of $1.028 \text{ V/\AA}^{\circ}$ (which is slightly lower than the theoretical electric field calculated earlier using simple model), one extra order of Raman enhancement was achieved in addition to the enhancement from the gold atom attachment. This shows that build-in electric field can actually bridge the gap between high enhancement experimental observations and previous theoretical simulations. In fact, with an application of a high build-in field of $2.570 \text{ V/\AA}^{\circ}$ we achieved a 2~4 more orders of enhancement (please see supporting information), which points to the importance of a metal-molecular junction for the potential 10^{14} Raman enhancement.

Effect of direction of electric field

The intensity of a vibrational mode is proportional to the square of scalar product of the electric field and the dipole moment derivative of the mode ($d\bar{\mu}/dQ$) as $I \propto \left| \frac{d\bar{\mu}}{dQ} \vec{E} \right|^2 = \left| \frac{d\bar{\mu}}{dQ} \right|^2 |\vec{E}|^2 \cos^2 \beta$ [102], where β is the angle between electric field, \vec{E} and $d\bar{\mu}/dQ$. This shows that there is a strong dependence of Raman peak intensity to direction of electric field. In fact, in our DFT simulation, we observed that applying electric field in a direction parallel to the aromatic ring decreases the SERS enhancement as shown in Fig. 8. Further, aligning the electric field in Gold-Sulfur bond direction improved the signals. Finally, with the application of electric field perpendicular to the aromatic ring further increases SERS enhancement. This concludes that molecular orientations relative to built-in electric field in the junction dictate in this enhancement mechanism. The reorientation of molecule relative to surface due to changes in the electrode potential has been reported by Moskovits et al. [103]. Subsequent detailed study using high resolution electron energy loss spectroscopy (HREELS) by Wan et al. [50] for benzenethiol adsorption to Au (111) surface further confirms our hypothesis that molecule orientation relative to built-in electric field is playing an important role for the charge transfer mechanism in SERS.

Vibrational shift in SERS

In general, all the Raman peak positions in SERS spectra are never consistent with those of original Raman spectra [44, 104-107]. The frequency shifts of seven commonly observed modes in benzenethiol are compared to experimental SERS and DFT calculated data in Table 1. The values of the vibrational frequencies (termed as Freq. PhSH) are taken for neat benzenethiol from our experiments [93]. The vibrational band at $\omega_1 = 1005 \text{ cm}^{-1}$ is assigned to the ring breathing mode (β_{CCC}) (please see supporting information for the movies), and the band at $\omega_2 = 1032 \text{ cm}^{-1}$ corresponds to a ring deformation mode (β_{CH}). The C–S stretching mode ($\beta_{\text{CCC}} + \nu_{\text{CS}}$), is given at $\omega_3 = 1099 \text{ cm}^{-1}$ while the computed Raman band at $\omega_4 = 1584 \text{ cm}^{-1}$ is associated with a totally symmetric ring stretching mode (ν_{CC}). The other important modes are $\omega_5 = 420 (\nu_{\text{CS}} + \beta_{\text{CCC}})$, $\omega_6 = 705 (\beta_{\text{CCC}} + \nu_{\text{CS}})$ and 922 cm^{-1} (β_{SH}). Note that the 922

cm^{-1} generally disappears in SERS spectra due to thiolate bond formation. The large shift in the C-S stretching mode (1099 cm^{-1}) in SERS can be attributed to the proximity effect as the vibrational mode is strongly enhanced by the interaction with Au cluster [44].

As described above, the C-C bond stretch mode on the aromatic ring was observed at 1584 cm^{-1} in the original Raman spectrum which is consistent with our DFT simulation results. In a parallel SERS experiment reported in the paper [93, 107], the SERS peak for the same mode was observed at 1573 cm^{-1} . Apparently the Raman peak position shifts in the SERS spectrum in comparison with the original Raman spectrum. Although with only one gold atom conjugation there is a shift of Raman peak position in our simulation from 1584 cm^{-1} to 1560 cm^{-1} , but it is not consistent with the experimental observation, where it shifts to 1573 cm^{-1} . On the other hand, with including the build-in electric field effect (1.028 V/\AA) in our DFT simulation we observed the SERS peak at 1573 cm^{-1} which exactly matches with the experimental observation (Fig. 9). Similarly, the large enhancement of 420 cm^{-1} peak ($\beta\text{CCC}+\nu\text{CS}$), is obtained in our simulation only after taking into account of the metal molecular Schottky junction (Fig. 9), which is also consistent with the experimental observations [93, 107] and theoretical prediction [44].

Finally, Fig. 10 shows the vibrational shift observed in our DFT simulation when we applied electric field of different magnitude perpendicular to the ring structure. The plot is shown for a characteristic peak of 1573 cm^{-1} and corresponds to the case when benzenethiol molecule is not attached to any gold atom (so this will discount any interference of charge transfer from gold cluster and thus represents the effect purely due to electric field only). We observed a closely linear fall of vibrational shift of ring stretching mode (ν_{CC}) with electric field and the stark tuning rate was calculated to be $13.2 \text{ cm}^{-1}/(\text{V/\AA})$. In fact this value is very close to the vibrational shift observed (which ranges from $\sim 10\text{-}13 \text{ cm}^{-1}$) in many SERS experiments for this particular characteristics peak [105-107]. In spite of not having enough statistics to prove our hypothesis, the results clearly points to a possible role of electric field of strength $\sim 1 \text{ V/\AA}$. In addition, though the accuracy and precision of DFT is in doubt [108], still the correct trend of vibrational shift can be inferred from the present simulation. Since the inclusion of build-in electric

field contribution leads to correct prediction of Raman peak shifts, we believe that the build-in electric field is playing an important role in SERS process.

Conclusion

In summary, we have performed a quantum mechanical simulation to study the effect of build-in electric field due to a Schottky barrier formed between the molecule monolayer and metallic SERS substrate. We found that the application of build-in electric field changes the bond lengths and dihedral angles which lead to an alteration in the dipole moment. Further, this build-in field also causes a modification in the polarizability and polarizability derivatives of the molecule, which are mainly responsible for the drastic change in scattering cross-section observed in SERS. We have also shown that the order of enhancement that can be obtained in Raman scattering cross section is highly dependent on the direction of the build-in electric field. This help to explain the non-repeatability of many SERS experiments. Finally, by adding strong electrostatic build-in field can result in 2-4 more orders of enhancement in SERS for Benzenethiol molecules.

Acknowledgements

This work performed under the auspices of the DOE by LLNL under Contract No. DE-AC52-07NA27344. We thank Prof. Nick Fang, Mechanical Science and Engineering, University of Illinois, Urbana-Champaign, for the valuable discussions and suggestions.

References and notes

- (1) Fleischmann, M.; Hendra, P. J.; McQuillan, A. J. Raman Spectra of Pyridine Adsorbed at a Silver Electrode. *Chemical Physics Letters* **1974**, *26*, 163-166.
- (2) Jeanmaire, D. L.; Van Duyne, R. P. Surface Raman Spectroelectrochemistry: Part I. Heterocyclic, Aromatic, and Aliphatic Amines Adsorbed on the Anodized Silver Electrode. *J Electroanal Chem* **1977**, *84*, 1-20.
- (3) Albrecht, M. G.; Creighton, J. A. Anomalously Intense Raman Spectra of Pyridine at a Silver Electrode. *J. Am. Chem. Soc.* **1977**, *99*, 5217.
- (4) Cotton, T. M.; Schultz, S. G.; Van Duyne, R. P. Surface-Enhanced Resonance Raman Scattering from Cytochrome c and Myoglobin Adsorbed on a Silver Electrode. *J. Am. Chem. Soc.* **1980**, *102*, 7962.
- (5) Nie, S.; Emory, S. R. Probing Single Molecules and Single Nanoparticles by Surface-Enhanced Raman Scattering. *Science* **1997**, *275*, 1102-1106.
- (6) Kneipp, K.; Wang, Y.; Kneipp, H.; Perelman, L. T.; Itzkan, I.; Dasari, R. R.; Feld, M. S. Single Molecule Detection using Surface-Enhanced Raman Scattering (SERS). *Phys. Rev. Lett.* **1997**, *78*.
- (7) Lyandres, O.; Shah, N. C.; Yonzon, C. R.; Walsh, J. T.; Glucksberg, M. R.; Van Duyne, R. P. Real-Time Glucose Sensing by Surface-Enhanced Raman Spectroscopy in Bovine Plasma Facilitated by a Mixed Decanethiol/Mercaptohexanol Partition Layer. *Anal. Chem.* **2005**, *77*, 6139.
- (8) Lyandres, O.; Yuen, J. M.; Shah, N. C.; VanDuyne, R. P.; Walsh, J. J. T.; Glucksberg, M. R. Progress Toward an in Vivo Surface-Enhanced Raman Spectroscopy Glucose Sensor. *Diabetes technology therapeutics* **2008**, *10*, 257.
- (9) Yonzon, C.; Lyandres, O.; Shah, N.; Dieringer, J.; Van Duyne, R. Glucose Sensing with Surface-Enhanced Raman Spectroscopy. **2006**, *103*, 367.

- (10) Zamarion, V. M.; Timm, R. A.; Araki, K.; Toma, H. E. Ultrasensitive SERS Nanoprobes for Hazardous Metal Ions Based on Trimercaptotriazine-Modified Gold Nanoparticles. *Inorg. Chem.* **2008**, *47*, 2934.
- (11) Zhang, X.; Shah, N. C.; Van Duyne, R. P. Sensitive and Selective chem/bio Sensing Based on Surface-Enhanced Raman Spectroscopy (SERS). *Vibrational Spectroscopy* **2006**, *42*, 2-8.
- (12) Qian, X.; Peng, X.; Ansari, D. O.; Yin-Goen, Q.; Chen, G. Z.; Shin, D. M.; Yang, L.; Young, A. N.; Wang, M. D.; Nie, S. In Vivo Tumor Targeting and Spectroscopic Detection with Surface-Enhanced Raman Nanoparticle Tags. *Nature Biotechnology* **2008**, *26*, 90.
- (13) Fujita, K.; Ishitobi, S.; Hamada, K.; Smith, N. I. Time-Resolved Observation of Surface-Enhanced Raman Scattering from Gold Nanoparticles during Transport through a Living Cell. *J. Biomed. Opt.* **2009**, *14*, 024038.
- (14) Lombardi, J. R.; Birke, R. L. A Unified View of Surface-Enhanced Raman Scattering. *Accounts of Chemical Research* **2009**, *42*, 742.
- (15) Moskovits, M. Surface Roughness and the Enhanced Intensity of Raman Scattering by Molecules Adsorbed on Metals. *J. Chem. Phys.* **1978**, *69*, 4159.
- (16) Lombardi, J. R.; Birke, R. L.; Lu, T.; Xu, J. Charge-Transfer Theory of Surface Enhanced Raman Spectroscopy: Herzberg-Teller Contributions. *J. Chem. Phys.* **1986**, *84*, 4174.
- (17) Lombardi, J. R.; Birke, R. L. A Unified Approach to Surface-Enhanced Raman Scattering. *J. Phys. Chem. C*, **2008**, *112*, 5617.
- (18) Campion, A.; Kambhampati, P. Surface-Enhanced Raman Scattering. *Chem. Soc. Rev.* **1998**, *27*, 241.
- (19) Kneipp, K.; Kneipp, H.; Itzkan, I.; Dasari, R. R.; Feld, M. S. Surface-Enhanced Raman Scattering and Biophysics. *Journal of physics. Condensed matter* **2002**, *14*, R597.

- (20) Furtak, T. E.; Macomber, S. H. Voltage-Induced Shifting of Charge-Transfer Excitations and their Role in Surface-Enhanced Raman Scattering. *Chemical Physics Letters* **1983**, *95*, 328-332.
- (21) Pockrand, I.; Otto, A. Surface Enhanced and Disorder Induced Raman Scattering from Silver Films. *Solid State Commun.* **1981**, *37*, 109-112.
- (22) Lombardi, J. R.; Birke, R. L.; Sanchez, L. A.; Bernard, I.; Sun, S. C. The Effect of Molecular Structure on Voltage Induced Shifts of Charge Transfer Excitation in Surface Enhanced Raman Scattering. *Chemical Physics Letters* **1984**, *104*, 240-247.
- (23) Burstein, E.; Chen, Y. J.; Chen, C. Y.; Lundquist, S.; Tosatti, E. "Giant" Raman Scattering by Adsorbed Molecules on Metal Surfaces. *Solid State Commun.* **1979**, *29*, 567-570.
- (24) Persson, B. N. J. On the Theory of Surface-Enhanced Raman Scattering. *Chemical Physics Letters* **1981**, *82*, 561-565.
- (25) Gersten, J. I.; Birke, R. L.; Lombardi, J. R. Theory of Enhanced Light Scattering from Molecules Adsorbed at the Metal-Solution Interface. *Phys. Rev. Lett.* **1979**, *43*, 147– 150.
- (26) Moskovits, M. Surface-Enhanced Spectroscopy. *Reviews of modern physics* **1985**, *57*, 783.
- (27) Otto, A.; Mrozek, I.; Grabhorn, H.; Akemann, W. Surface-Enhanced Raman Scattering. *Journal of Physics: Condensed Matter* **1992**, *4*, 1143.
- (28) Jin, R. Nanoparticle Clusters Light Up in SERS. *Angewandte Chemie (International ed.in English)* **2010**, *49*, 2826 – 2829.
- (29) Sun, M.; Li, Z.; Liu, Y.; Xu, H. Direct Visual Evidence for Chemical Mechanisms of SERRS Via Charge Transfer in Au₂₀-Pyrazine-Au₂₀ Junction. *J. Raman Spectrosc.* **2009**, *40*, 1942.
- (30) Xu, H. X.; Bjerneld, E. J.; Käll, M.; Börjesson, L. Spectroscopy of Single Hemoglobin Molecules by Surface Enhanced Raman Scattering. *Phys. Rev. Lett.* **1999**, *83*.
- (31) General Discussion. *Faraday Discuss.* **2006**, *132*, 227 - 247.

- (32) Lazorenko-Manevich, R. M. Adatom Hypothesis as a Predominant Mechanism of Surface Enhanced Raman Scattering: A Review of Experimental Argumentation. *Russian J. Electrochem.* **2005**, *41*, 799.
- (33) Otto, A.; Timper, J.; Billmann, J.; Kovacs, G.; Pockrand, I. Surface Roughness Induced Electronic Raman Scattering. *Surf. Sci.* **1980**, *92*, L55.
- (34) Morton, S. M.; Jensen, L. Understanding the Molecule-Surface Chemical Coupling in SERS. *J. Am. Chem. Soc.* **2009**, *131*, 4098.
- (35) Udagawa, M.; Chou, C.; Hemminger, J. C.; Ushioda, S. Raman Scattering Cross Section of Adsorbed Pyridine Molecules on a Smooth Silver Surface. *Phys. Rev. B* **1981**, *23*.
- (36) Jiang, X.; Campion, A. Chemical Effects in Surface-Enhanced Raman Scattering: Pyridine Chemisorbed on Silver Adatoms on Rh (100). *Chemical Physics Letters* **1987**, *140*, 95-100.
- (37) Zhao, L. L.; Jensen, L.; Schatz, G. C. Surface-Enhanced Raman Scattering of Pyrazine at the Junction between Two Ag₂₀ Nanoclusters. *J. Am. Chem. Soc.* **2006**, *6*, 1234.
- (38) Nikoobakht, B.; Wang, J.; El-Sayed, M. A. Surface-Enhanced Raman Scattering of Molecules Adsorbed on Gold Nanorods: Off-Surface Plasmon Resonance Condition. *Chemical Physics Letters* **2002**, *366*, 17-23.
- (39) Fromm, D. P.; Sundaramurthy, A.; Kinkhabwala, A.; Schuck, P. J.; Kino, G. S.; Moerne, W. E. Exploring the Chemical Enhancement for Surface-Enhanced Raman Scattering with Au Bowtie Nanoantennas. *J. Chem. Phys.* **2006**, *124*, 061101.
- (40) Peyser-Capadona, L.; Zheng, J.; Gonzalez, J. I.; Lee, T. H.; Patel, S. A.; Dickson, R. M. Nanoparticle-Free Single Molecule Anti-Stokes Raman Spectroscopy. *Phys. Rev. Lett.* **2005**, *94*, 058301.

- (41) Zheng, J.; Ding, Y.; Tian, B.; Wang, Z. L.; Zhuang, X. Luminescent and Raman Active Silver Nanoparticles with Polycrystalline Structure. *J. Am. Chem. Soc.* **2008**, *130*, 10473.
- (42) Yang, L.; Jiang, X.; Ruan, W.; Zhao, B.; Xu, W.; Lombardi, J. R. Observation of Enhanced Raman Scattering for Molecules Adsorbed on TiO₂ Nanoparticles: Charge-Transfer Contribution. *J. Phys. Chem. C* **2008**, *112*, 20098.
- (43) Jensen, L.; Aikens, C. M.; Schatz, G. C. Electronic Structure Methods for Studying Surface-Enhanced Raman Scattering. *Chem. Soc. Rev.* **2008**, *37*, 1061.
- (44) Saikin, S. K.; Olivares-Amaya, R.; Rappoport, D.; Stopa, M.; Aspuru-Guzik, A. On the Chemical Bonding Effects in the Raman Response: Benzenethiol Adsorbed on Silver Clusters. *Physical chemistry chemical physics* **2009**, *11*, 9401.
- (45) Otto, A. The Chemical (Electronic) Contribution to Surface-Enhanced Raman Scattering. *J. Raman Spectrosc.* **2005**, *36*, 497.
- (46) Aroca, R. F.; Clavijo, R. E.; Halls, M. D.; Schlegel, H. B. Surface-Enhanced Raman Spectra of Phthalimide. Interpretation of the SERS Spectra of the Surface Complex Formed on Silver Islands and Colloids. *J. Phys. Chem. A* **2000**, *104*, 9505.
- (47) Jensen, L.; Zhao, L. L.; Autschbach, J.; Schatz, G. C. Theory and Method for Calculating Resonance Raman Scattering from Resonance Polarizability Derivatives. *J. Chem. Phys.* **2005**, *123*, 174110.
- (48) Jensen, L.; Zhao, L. L.; Schatz, G. C. Size-Dependence of the Enhanced Raman Scattering of Pyridine Adsorbed on Ag_n (n= 2-8, 20) Clusters. *The Journal of Physical Chemistry. C* **2007**, *111*, 4756.
- (49) Nara, J.; Higai, S.; Morikawa, Y.; Ohno, T. Density Functional Theory Investigation of Benzenethiol Adsorption on Au (111). *J. Chem. Phys.* **2004**, *120*, 6705.

- (50) Wan, L.; Terashima, M.; Noda, H.; Osawa, M. Molecular Orientation and Ordered Structure of Benzenethiol Adsorbed on Gold (111). *J. Phys. Chem. B* **2000**, *104*, 3569.
- (51) Vivoni, A.; Birke, R. L.; Foucault, R.; Lombardi, J. R. Ab Initio Frequency Calculations of Pyridine Adsorbed on an Adatom Model of a SERS Active Site of a Silver Surface. *J. Phys. Chem. B* **2003**, *107*, 5557.
- (52) Wu, D. Y.; Duan, S.; Ren, B.; Tian, Z. Q. Density Functional Theory Study of Surface-Enhanced Raman Scattering Spectra of Pyridine Adsorbed on Noble and Transition Metal Surfaces. *J. Raman Spectrosc.* **2005**, *36*, 533.
- (53) Cardini, G.; Miranda, M. M. Density Functional Study on the Adsorption of Pyrazole Onto Silver Colloidal Particles. *The Journal of Physical Chemistry.B* **2002**, *106*, 6875.
- (54) Wu, D. Y.; Ren, B.; Jiang, Y. X.; Xu, X.; Tian, Z. Q. Density Functional Study and Normal-Mode Analysis of the Bindings and Vibrational Frequency Shifts of the Pyridine-M (M = Cu, Ag, Au, Cu⁺, Ag⁺, Au⁺, and Pt) Complexes. *The Journal of Physical Chemistry.A* **2002**, *106*, 9042.
- (55) Cardini, G.; Muniz-Miranda, M.; Pagliai, M.; Schettino, V. A Density Functional Study of the SERS Spectra of Pyridine Adsorbed on Silver Clusters. *Theor. Chem. Acc.* **2007**, *117*, 458.
- (56) Johansson, P. Illustrative Direct Ab Initio Calculations of Surface Raman Spectra. *Physical chemistry chemical physics* **2005**, *7*, 475.
- (57) Wu, D. Y.; Hayashi, M.; Lin, S. H.; Tian, Z. Q. Theoretical Differential Raman Scattering Cross-Sections of Totally-Symmetric Vibrational Modes of Free Pyridine and pyridine-metal Cluster Complexes. *Spectrochimica Acta Part A: Molecular and Biomolecular Spectroscopy* **2004**, *60*, 137-146.
- (58) Lambert, D. K. Vibrational Stark Effect of Adsorbates at Electrochemical Interfaces. *Electrochim. Acta* **1996**, *41*, 623-630.

- (59) Lambert, D. K. Electric Field Induced Change of Adsorbate Vibrational Line Strength. *J. Chem. Phys.* **1991**, *94*, 6237.
- (60) Nart, F. C.; Iwasita, T. Static Field Effect on the Band Intensity of Adsorbed Sulfate Ions. *Electrochim. Acta* **1996**, *41*, 631-636.
- (61) Pomfret, M. B.; Pietron, J. J.; Owrutsky, J. C. Measurement of Benzenethiol Adsorption to Nanostructured Pt, Pd, and PtPd Films using Raman Spectroelectrochemistry. *Langmuir* **2010**, *26*, 6809.
- (62) Gomez, R.; Perez, J. M.; Gullon, J. S.; Montiel, V.; Aldaz, A. In Situ Surface Enhanced Raman Spectroscopy on Electrodes with Platinum and Palladium Nanoparticle Ensembles. *The journal of physical chemistry.B* **2004**, *108*, 9943.
- (63) Sawai, Y.; Takimoto, B.; Nabika, H.; Ajito, K.; Murakoshi, K. Control of Near-Infrared Optical Response of Metal Nano-Structured Film on Glass Substrate for Intense Raman Scattering. *Faraday Discuss.* **2006**, *132*, 179.
- (64) Kilitziraki, M.; Moore, A. J.; Petty, M. C.; Bryce, M. R. Evaporated Thin Films of Tetrathiafulvalene Derivatives and their Charge-Transfer Complexes. *Thin Solid Films* **1998**, *335*, 209-213.
- (65) Geiser, U. *Toward crystal design in organic conductors and superconductors*; **1999**, Proceedings of the 28th International School of Crystallography, Erice, Italy, May 1999.
- (66) Horowitz, G. Organic Field-Effect Transistors. *Adv Mater* **1998**, *10*, 365.
- (67) Kymissis, I. In *Organic Field Effect Transistors*; Springer: 2009; Chap. 2.
- (68) Yamashita, Y. Organic Semiconductors for Organic Field-Effect Transistors. *Science and technology of advanced materials* **2009**, *10*, 024313.
- (69) Schottky, W. *Phs. Z* **1940**, *41*, 570.

- (70) Bardeen, J. Surface States and Rectification at a Metal Semi-Conductor Contact. *Physical review* **1947**, *71*, 717.
- (71) Heimel, G.; Romaner, L.; Zojer, E.; Bredas, J. The Interface Energetics of Self-Assembled Monolayers on Metals. *Accounts of Chemical Research* **2008**, *41*, 729.
- (72) Heimel, G.; Romaner, L.; Brédas, J.; Zojer, E. Organic/metal Interfaces in Self-Assembled Monolayers of Conjugated Thiols: A First-Principles Benchmark Study. *Surf. Sci.* **2006**, *600*, 4548-4562.
- (73) Heimel, G.; Romaner, L.; Bredas, J.; Zojer, E. Interface Energetics and Level Alignment at Covalent Metal-Molecule Junctions: π -Conjugated Thiols on Gold. *Phys. Rev. Lett.* **2006**, *96*, 196806.
- (74) Ishii, H.; Sugiyama, K.; Ito, E.; Seki, K. Energy Level Alignment and Interfacial Electronic Structures at organic/metal and organic/organic Interfaces. *Adv Mater* **1999**, *11*, 605.
- (75) Campbell, I. H.; Davids, P. S.; Smith, D. L.; Barashkov, N. N.; Ferraris, J. P. The Schottky Energy Barrier Dependence of Charge Injection in Organic Light-Emitting Diodes. *Appl. Phys. Lett.* **1998**, *72*, 1863.
- (76) Betti, M. G.; Kanjilal, A.; Mariani, C.; Vazquez, H.; Dappe, Y. J.; Ortega, J.; Flores, F. Barrier Formation at Organic Interfaces in a Cu (100)-Benzenethiolate-Pentacene Heterostructure. *Phys. Rev. Lett.* **2008**, *100*, 027601.
- (77) de Boer, B.; Hadipour, A.; Mandoc, M. M.; van Woudenberg, T.; Blom, P. W. M. Tuning of Metal Work Functions with Self-Assembled Monolayers. *Adv Mater* **2005**, *17*, 621.
- (78) Chen, J.; Reed, M. A.; Rawlett, A. M.; Tour, J. M. Large on-Off Ratios and Negative Differential. *Science* **1999**, *286*, 1550.

- (79) Whelan, C. M.; Smyth, M. R.; Barnes, C. J. HREELS, XPS, and Electrochemical Study of Benzenethiol Adsorption on Au(111). *Langmuir* **1999**, *15*, 126.
- (80) Pauling, L. The Nature of the Chemical Bond. Application of Results obtained from the Quantum Mechanics and from a Theory of Paramagnetic Susceptibility to the Structure of Molecules. *J. Am. Chem. Soc.* **1931**, *53*, 1367. Also in Pauling, L. The nature of the Chemical Bond, 3rd ed.; Cornell University Press: New York (1960).
- (81) Valiskó, M.; Boda, D. Relative Permittivity of Polar Liquids. Comparison of Theory, Experiment, and Simulation. *The journal of physical chemistry.B* **2005**, *109*, 6355.
- (82) Peisert, H.; Knupfer, M.; Fink, J. Energy Level Alignment at organic/metal Interfaces: Dipole and Ionization Potential. *Appl. Phys. Lett.* **2002**, *81*, 2400.
- (83) Nam, P. C.; Nguyen, M. T.; Chandra, A. K. Theoretical Study of the Substituent Effects on the S-H Bond Dissociation Energy and Ionization Energy of 3-Pyridinethiol: Prediction of Novel Antioxidant. *J. Phys. Chem. A* **2006**, *110*, 10911.
- (84) Ionization potential of Benzenethiol.
<http://www.bis.fm/assets/documents/faxdatasheets/Ion%20Science%20PhoCheck+2000%2010.6eV%20Gas%20Detection%20Table.pdf> (accessed 07/09, 2010).
- (85) Sze, S. M. In *Physics of Semiconductor Devices*; John Wiley Sons, Inc.: Hoboken, 2007; 2nd ed.
- (86) Yokota, K.; Taniguchi, M.; Kawai, T. Metal–Molecule Interfaces Formed by Noble–Metal–Chalcogen Bonds for Nanoscale Molecular Devices. *J. Phys. Chem. C* **2010**, *114*, 4050.
- (87) Braun, S.; Salaneck, W. R.; Fahlman, M. Energy-Level Alignment at organic/metal and organic/organic Interfaces. *Adv Mater* **2009**, *21*, 1450.
- (88) Tian, W.; Datta, S.; Hong, S.; Reifengerger, R.; Henderson, J. I.; Kubiak, C. P. Conductance Spectra of Molecular Wires. *J. Chem. Phys.* **1998**, *109*, 2874.

- (89) ADF: Amsterdam Density Functional software. <http://www.scm.com>.
- (90) Velde, te. G.; Bickelhaupt, F. M.; Baerends, E. J.; Guerra, C. F.; van Gisbergen, S. J. A.; Snijders, J. G.; Ziegler, T. Chemistry with ADF. *Journal of computational chemistry* **2001**, *22*, 931.
- (91) Becke, A. D. Density-Functional Exchange-Energy Approximation with Correct Asymptotic Behavior. *Physical review.A, Atomic, molecular, and optical physics* **1988**, *38*, 3098.
- (92) Perdew, J. P. Density-Functional Approximation for the Correlation Energy of the Inhomogeneous Electron Gas. *Phys. Rev. B* **1986**, *33*.
- (93) Gartia, M.R.; Xu, Z.; Behymer, E.; Nguyen, H.; Larson, C.; Bond, T.C.; Liu, G.L. Rigorous Surface Enhanced Raman Spectral Characterization of Large-Area Ultrahigh-Uniformity Silver-Coated Tapered Silica Nanopillar Arrays. *Nanotechnology* **2010** (submitted).
- (94) Etchegoin, P. G.; Galloway, C.; Le Ru, E. C. Polarization-Dependent Effects in Surface-Enhanced Raman Scattering (SERS). *Physical chemistry chemical physics* **2006**, *8*, 2624.
- (95) Arenas, J. F.; Woolley, M. S.; Otero, J. C.; Marcos, J. I. Charge Transfer Processes in Surface-Enhanced Raman Scattering. Franck-Condon Active Vibrations of Pyridine. *J. Phys. Chem.* **1996**, *100*, 3206.
- (96) Garraway, B.; Stenholm, S.; Suominen, K. A. Adventures in Wave Packet Land. *Physics World* **1993**, *46*.
- (97) van Gisbergen, S. J. A.; Snijders, J. G.; Baerends, E. J. Application of Time-Dependent Density Functional Response Theory to Raman Scattering. *Chemical Physics Letters* **1996**, *259*, 599-604.
- (98) Letardi, S.; Cleri, F. Interaction of Benzene Thiol and Thiolate with Small Gold Clusters. *J. Chem. Phys.* **2004**, *120*, 10062.
- (99) Lang, N. D.; Kohn, W. Theory of Metal Surfaces: Work Function. *Phys. Rev. B* **1971**, *3*.

- (100) Witte, G.; Lukas, S.; Bagus, P. S.; Woll, C. Vacuum Level Alignment at organic/metal Junctions: “Cushion” Effect and the Interface Dipole. *Appl. Phys. Lett.* **2005**, *87*, 263502.
- (101) Crispin, X.; Geskin, V.; Crispin, A.; Cornil, J.; Lazzaroni, R.; Salaneck, W. R.; Bredas, J. L. Characterization of the Interface Dipole at Organic/Metal Interfaces. *J. Am. Chem. Soc.* **2002**, *124*, 8141.
- (102) Allara, D. L.; Nuzzo, R. G. Spontaneously Organized Molecular Assemblies. 2. Quantitative Infrared Spectroscopic Determination of Equilibrium Structures of Solution-Adsorbed n –Alkanoic Acids on an Oxidized Aluminum Surface. *Langmuir* **1985**, *1*, 66.
- (103) Moskovits, M.; DiLella, D. P.; Maynard, K. J. Surface Raman Spectroscopy of a Number of Cyclic and Molecular Reorientation Aromatic Molecules Adsorbed on Silver: Selection Rules and Molecular Reorientation. *Langmuir* **1988**, *4*, 76.
- (104) Joo, T. H.; Kim, M. S.; Kim, K. Surface-Enhanced Raman Scattering of Benzenethiol in Silver Sol. *J. Raman Spectrosc.* **1987**, *18*, 57.
- (105) Biggs, K. B.; Camden, J. P.; Anker, J. N.; Duyne, R. P. V. Surface-Enhanced Raman Spectroscopy of Benzenethiol Adsorbed from the Gas Phase Onto Silver Film Over Nanosphere Surfaces: Determination of the Sticking Probability and Detection Limit Time. *J. Phys. Chem. A* **2009**, *113*, 4586.
- (106) Carron, K. T.; Hurley, L. G. Axial and Azimuthal Angle Determination with Surface-Enhanced Raman Spectroscopy: Thiophenol on Copper, Silver, and Gold Metal Surfaces. *J. Phys. Chem.* **1991**, *95*, 9984.
- (107) Aggarwal, R. L.; Farrar, L. W.; Diebold, E. D.; Polla, D. L. Measurement of the Absolute Raman Scattering Cross Section of the 1584-cm⁻¹ Band of Benzenethiol and the Surface-Enhanced Raman Scattering Cross Section Enhancement Factor for Femtosecond Laser-Nanostructured Substrates. *J. Raman Spectrosc.* **2009**, *40*, 1331.

(108) Cohen, A. J.; Sánchez, P. M.; Yang, W. Insights into Current Limitations of Density Functional Theory. *Science* **2008**, *321*, 792.

Figure Captions

Figure 1 (a) Schematic of metal-molecule Schottky barrier junction, the monolayer of benzenethiol molecules on gold cluster surface with perpendicular electric field orientation. (b) Schematic energy-band diagram of the Gold/Benzenethiol Schottky junction interface. E_F is the Fermi energy of metal, and I.P. is the ionization potential.

Figure 2 (a) Comparison of results obtained from DFT study with experiments. The spectra shown are for neat Raman (b) Comparison of SERS spectra of benzenethiol calculated by DFT simulation and obtained from experiment.

Figure 3 (a) The change in the C-S bond length and C-S-H dihedral angle as a function of electric field applied in X, Y and Z direction relative to the benzenethiol molecule has been shown. (b) The dihedral angle variation with build-in electric field perpendicular to the ring structure has been shown here. (c) The co-ordinates of each atom as found from the simulation have been plotted. The change in orientation of the molecule can be clearly seen. (d) The absolute polarizability derivative (modulus of the polarizability derivative) at two Raman peaks (403 cm^{-1} and 1573 cm^{-1}) is shown.

Figure 4 Sketch showing the schematic of charge transfer scheme explained in terms of HOMO and LUMO state of the molecule. The electric field changes the bond length and creates large dipole. Even though the molecule remains in the same electronics state (illustrated by the state in the same potential energy diagram), due to large dipole moment change, the Raman scattering cross section are enhanced. The attachment of gold atom creates an intermediate state in between ground state and excited state shown by molecule on a higher potential energy surface. The intermediate state coupled with large dipole moment change facilitates the charge transfer enhancement and that explains the enhanced Raman peaks with gold atoms. The combined effect of build-in electric field along with attach gold atoms can further elevate the molecule to a higher excited state.

Figure 5 The density of state plot for isolated benzenethiol (BT), the molecule adsorbed on one gold atom and when build-in electric field is applied to molecule adsorbed on the gold atom. Clearly the band gap has decreased with the adsorption and decreased further with the application of electric field. In addition, the degeneracy of number of states has increased as well, making it possible for better vibronic coupling and hence enhanced Raman scattering cross-section.

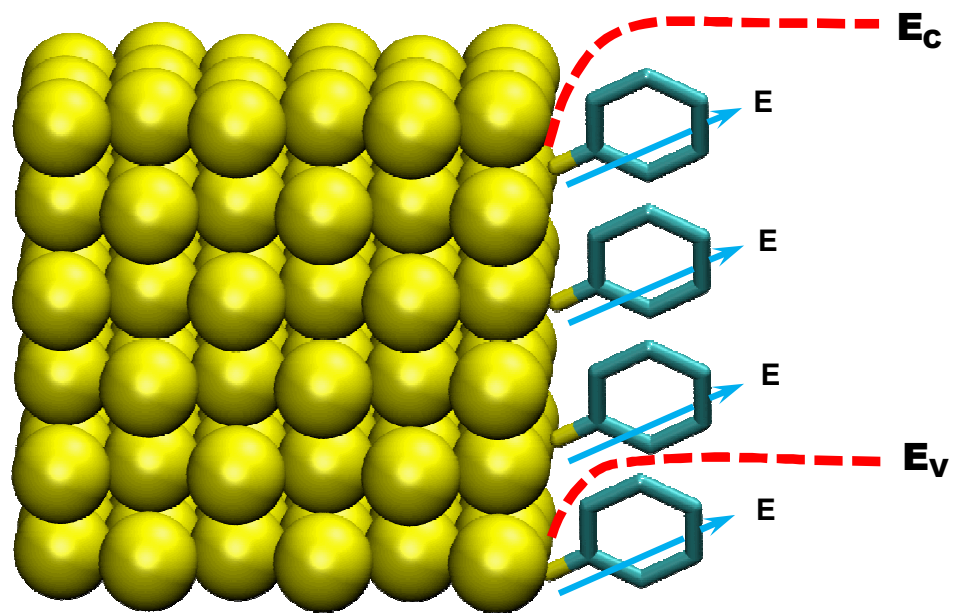
Figure 6 (a) Schematic energy-level diagram at a metal/organic molecule interface. Part (a) shows the position of the highest occupied molecular orbital (HOMO: H) and the lowest unoccupied molecular orbital (LUMO: L) of benzenethiol with respect to the Fermi level (E_F) of Au before contact. The hole injection barrier (HIB) and electron injection barrier (EIB) was calculated to be 2.06 and 2.04 eV respectively. After contact (b), the HIB and EIB can be reduced. (c) Model of a metal surface (square potential well in the absence of a surface dipole; (d) As electrons leak out of the potential well forming surface dipole (e) Upon interaction of the molecules, the electrons are pushed back into the metal, reducing the surface dipole and charge-carrier injection barriers.

Figure 7 Enhancement due to Gold-Benzenethiol Schottky barrier.

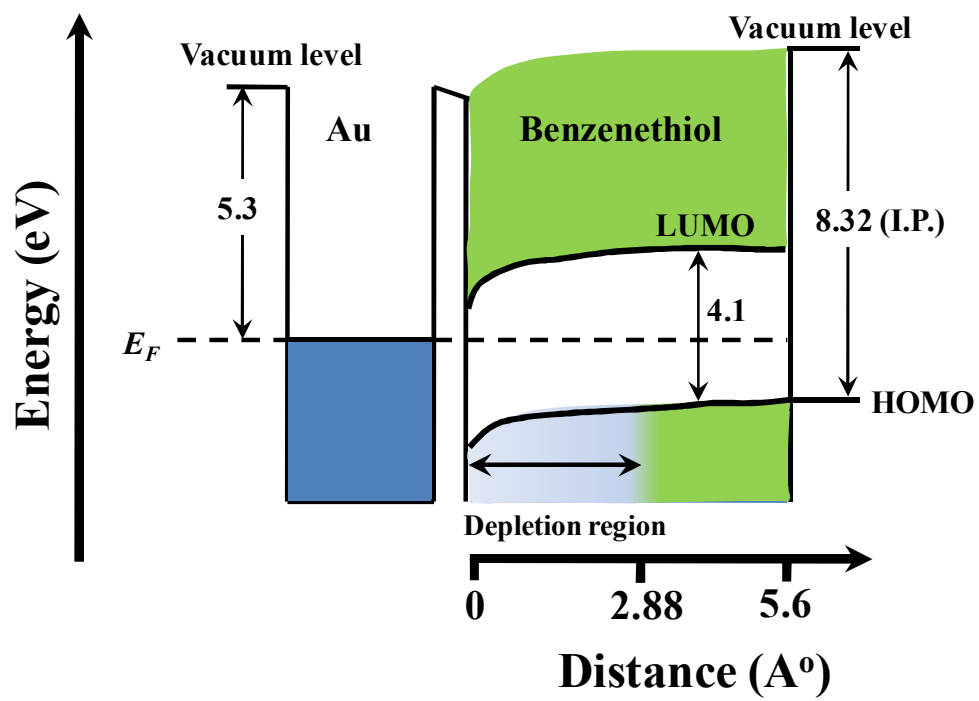
Figure 8 The effect of molecular orientation relative to build-in electric field. The application of build-in field in an unfavorable direction (parallel to the ring, X direction for the present case) results in a decrease of Raman peak intensity. On the other hand, applying the electric field in a favorable direction (perpendicular to the benzene ring structure, Y direction for the present case) leads to increase in Raman peak intensity.

Figure 9 Explanation for Raman peak shift. The inset shows the 420 cm^{-1} Raman peak position.

Figure 10 Effect of electric field on Raman vibrational shift

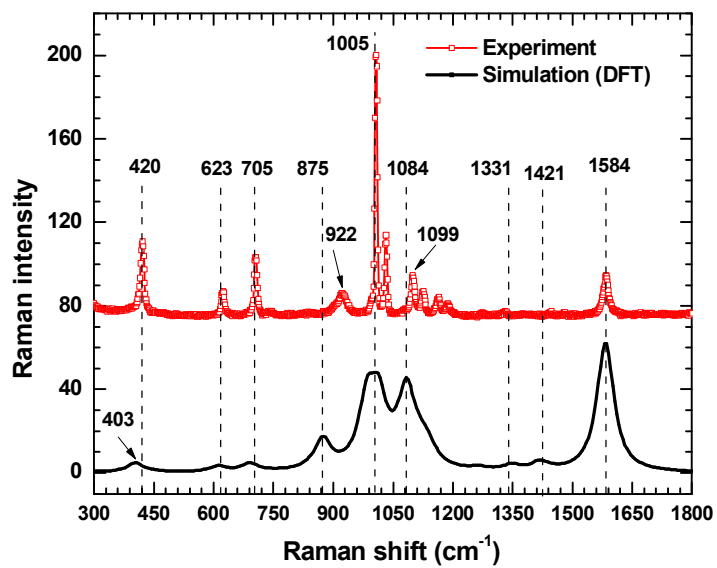


(a)

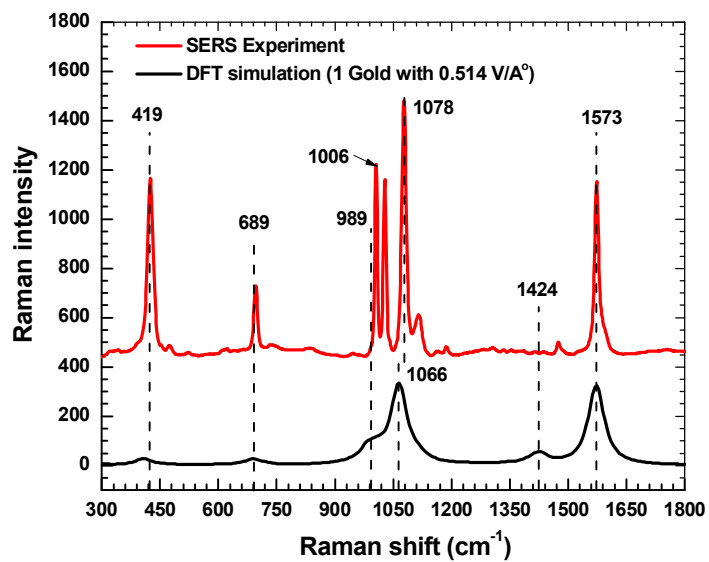


(b)

Figure 1

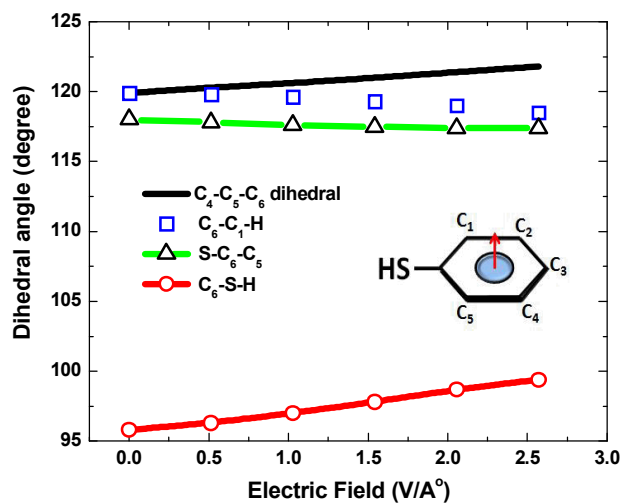
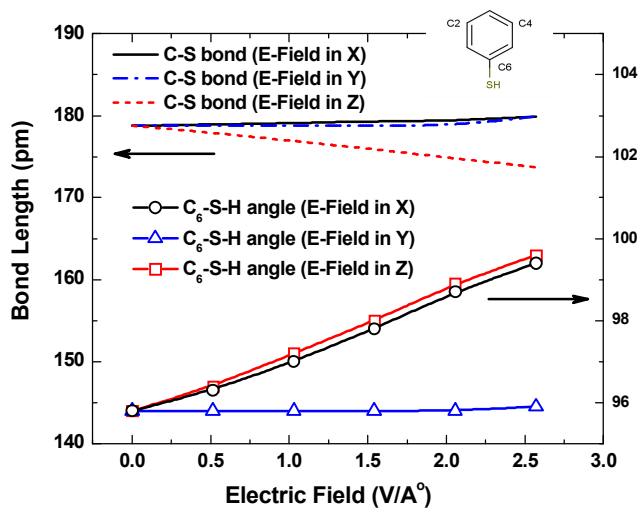


(a)



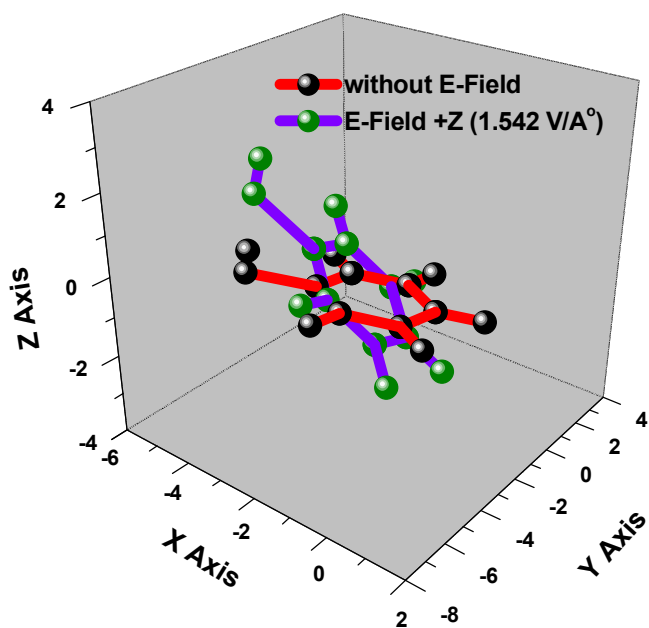
(b)

Figure 2

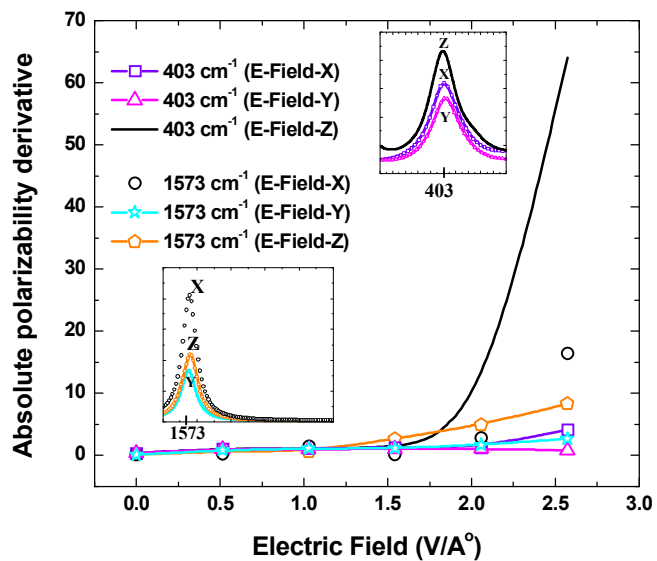


(a)

(b)



(c)



(d)

Figure 3

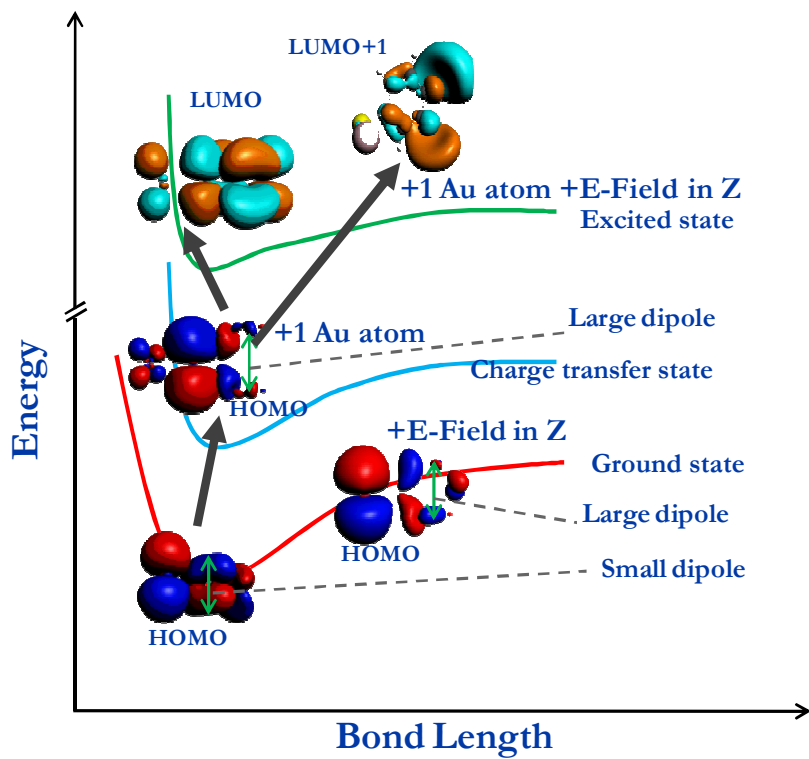


Figure 4

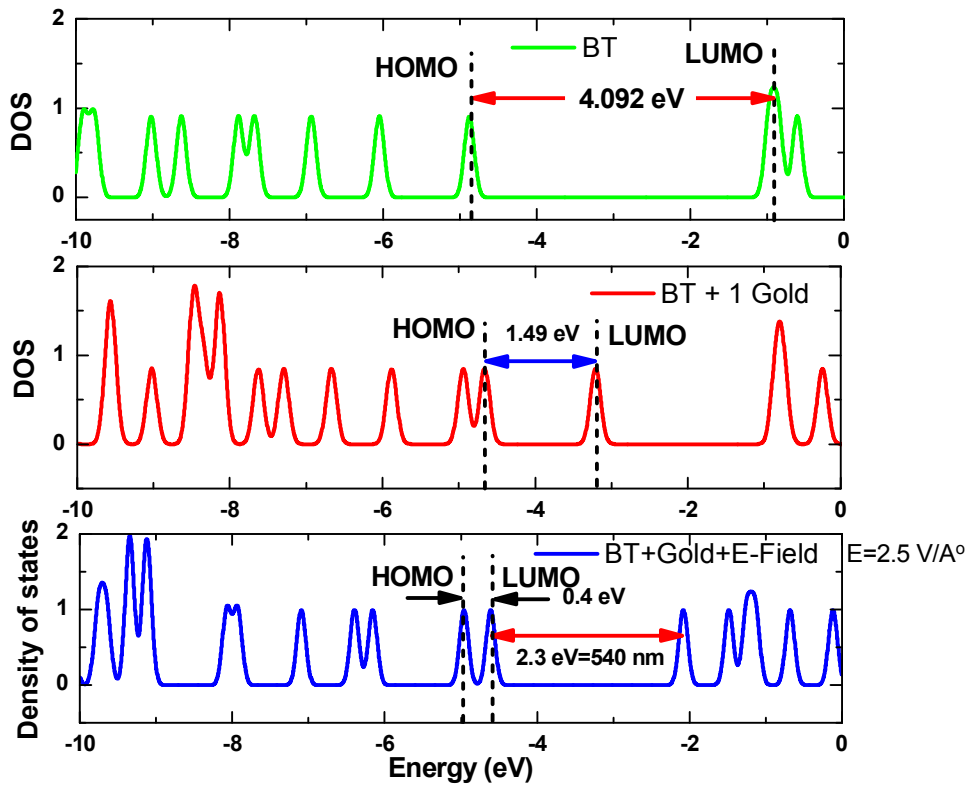
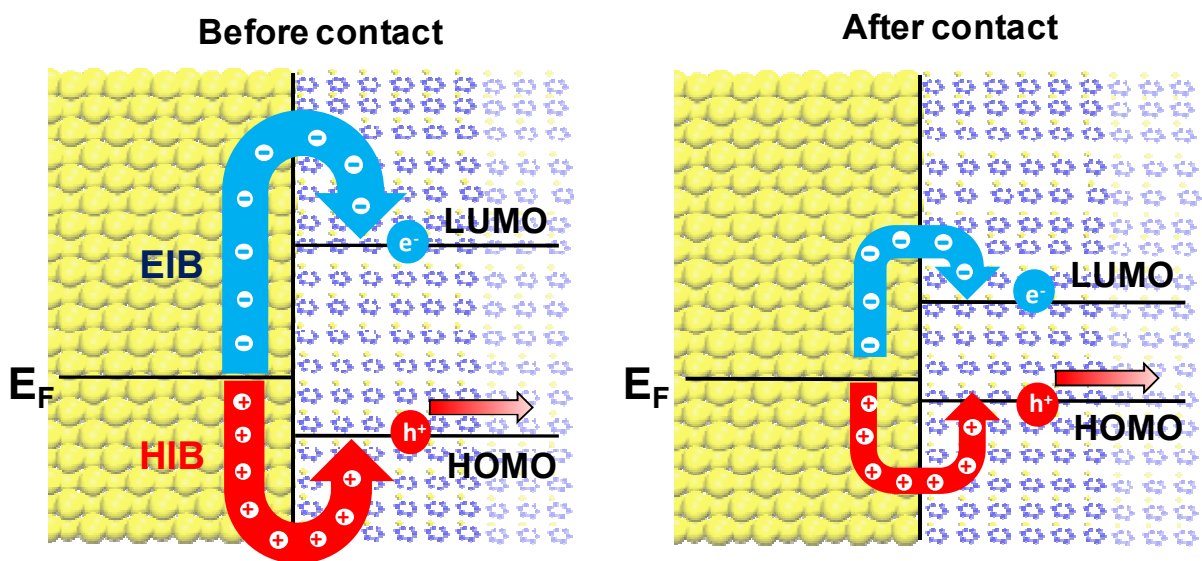
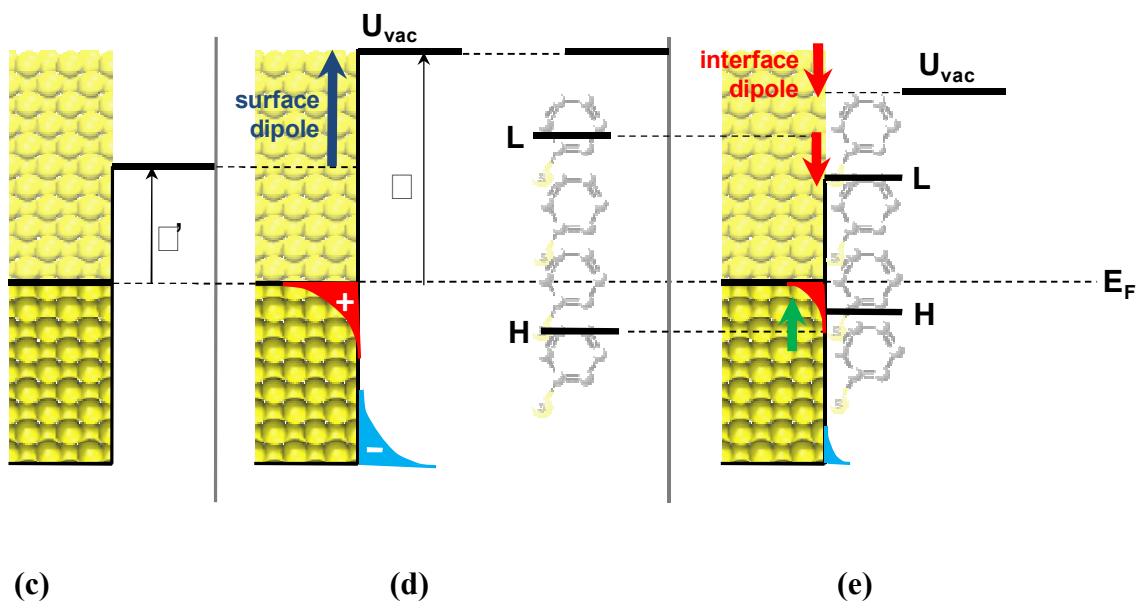


Figure 5



(a)

(b)



(c)

(d)

(e)

Figure 6

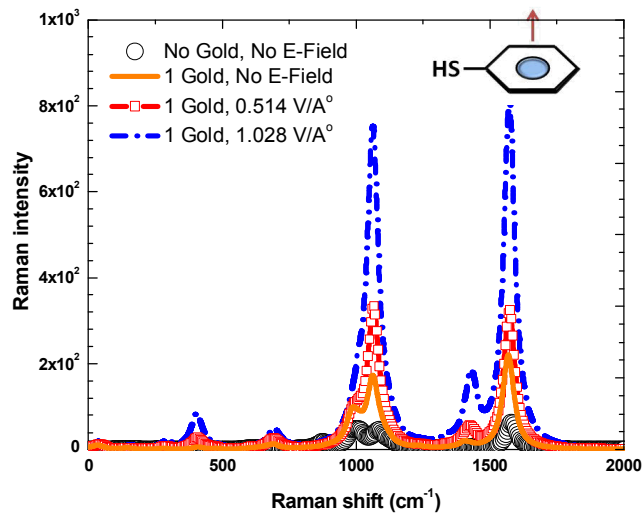
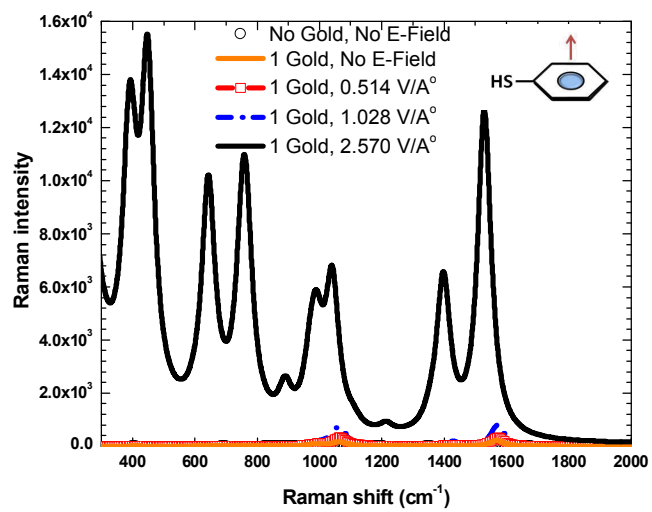


Figure 7

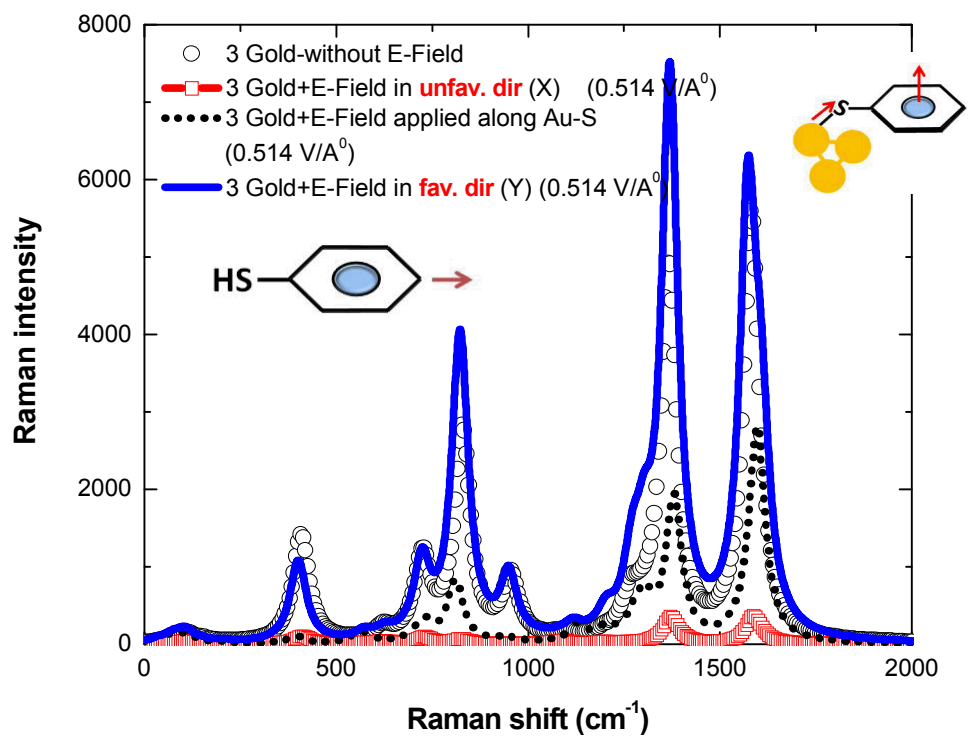


Figure 8

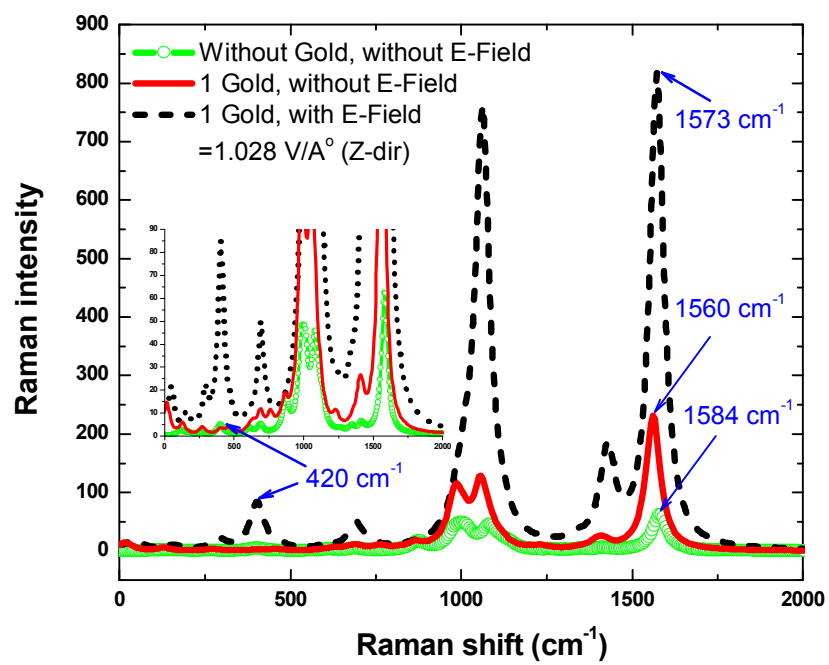


Figure 9

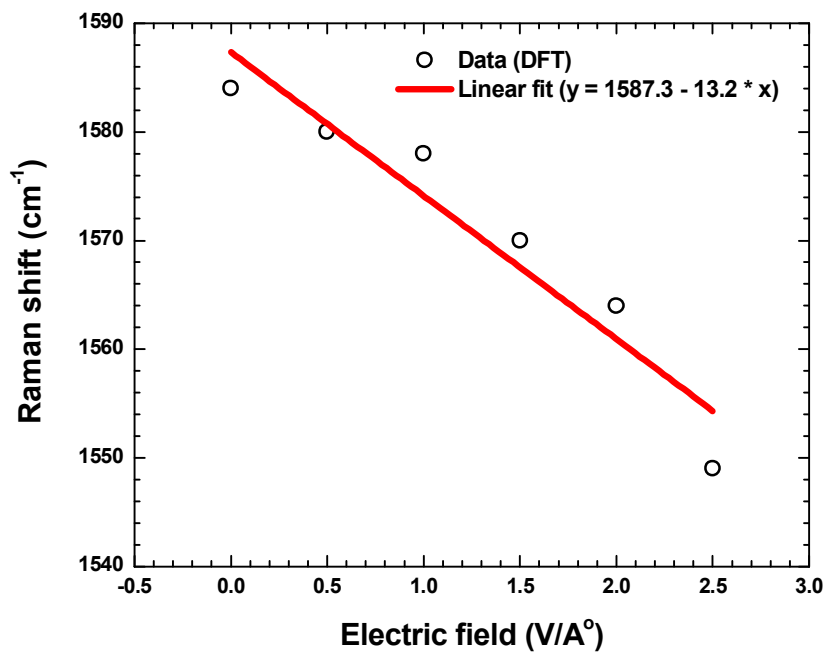


Figure 10

TABLE 1: The frequency shifts of benzenethiol Raman active vibrational modes due to binding to the metal and application of electric field (in DFT). The frequencies are given in cm^{-1} ; PhSH: Benzenethiol; The numbers in the bracket are the electric field value in $\text{V}/\text{\AA}^0$ applied in DFT simulations.

Mode	ω_1	ω_2	ω_3	ω_4	ω_5	ω_6	ω_7
Freq. PhSH	1005	1032	1099	1584	420	705	922
PhS-Ag (SERS)	1006	1028	1078	1573	425	696	---
PhSH-DFT	1002	---	1084	1584	403	691	875
PhSH-DFT (0.51)	991	---	1084	1580	403	696	882
PhSH-DFT (1.03)	992	---	1084	1578	403	691	882
PhSH-DFT (1.54)	989	---	1079	1570	400	676	882
PhSH-DFT (2.05)	981	---	1071	1564	426	631	869
PhSH-DFT (2.57)	---	1018	1047	1549	410	715	840
Ref-105	1003	1027	1076	1576	422	695	---
Ref-106	1004	1028	1077	1574	420	698	---
Ref-107	1003	1025	1073	1572	419	693	---
Ref- 44	1003	1024	1076	1574	419	697	907
PhS-Au ₁	---	---	1062	1560	403	693	---
PhS-Au1 (0.51)	---	---	1064	1571	408	693	---
PhS-Au1 (1.03)	988	---	1061	1573	409	693	---
PhS-Au1 (1.54)	983	---	1053	1563	409	693	---
PhS-Au1 (2.05)	979	---	1059	1551	382	712	---

PhS-Au1 (2.57)	1009	1035	1090	1571	408	713	922
----------------	------	------	------	------	-----	-----	-----
